Electronic supplementary information (ESI)

Cu-Fe-NH_2 based metal-organic framework nanosheets *via* drop-casting for highly efficient oxygen evolution catalysts durable at ultrahigh currents

Nabeen K. Shrestha*[a], Supriya A. Patil[a,b], Sangeun Cho[a], Yongcheol Jo[b], Hyungsang Kim*[a], Hyunsik Im*[a]

[a]Division of Physics and Semiconductor Science, Dongguk University, Seoul 04620, South Korea.

[b]Department Nanotechnology & Advanced Materials Engineering, Sejong University, Seoul 05006, South Korea.

[c]Quantum Functional Semiconductor Research Center (QSRC), Dongguk University, Seoul 04620, South Korea.

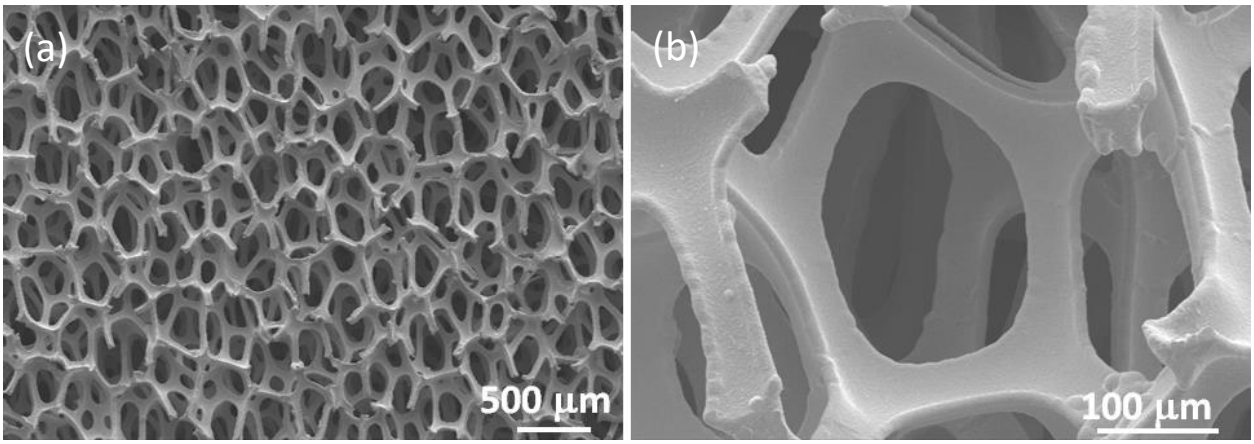

Fig. S1. (a) Low- and (b) high-magnification SEM images of Ni foam showing its highly porous three-dimensional network structure.

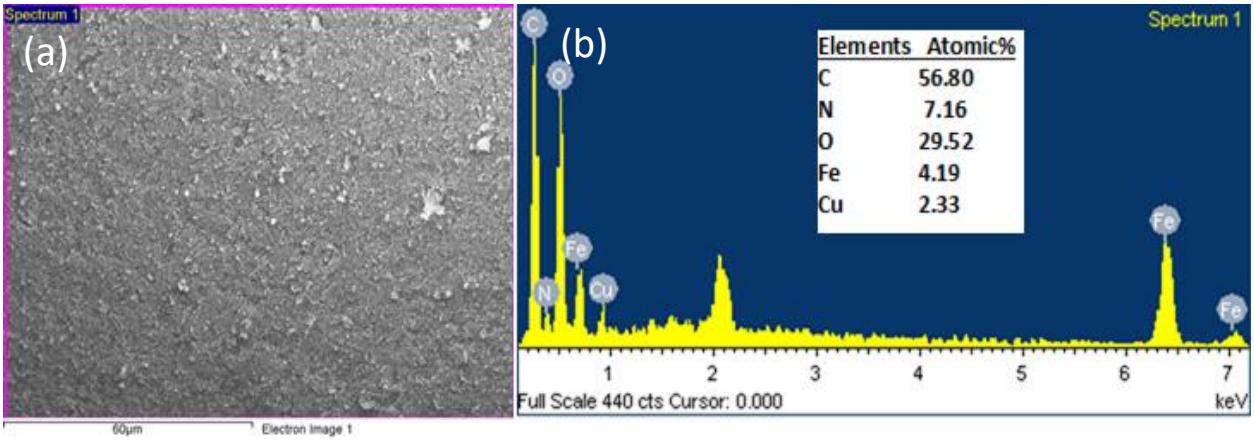

Fig. S2. (a) SEM image and (b) corresponding EDX spectrum of Cu-Fe-NH_2 MOF powder obtained from ink. Inset in "(b)" shows atomic ratios of various constituents of MOF.

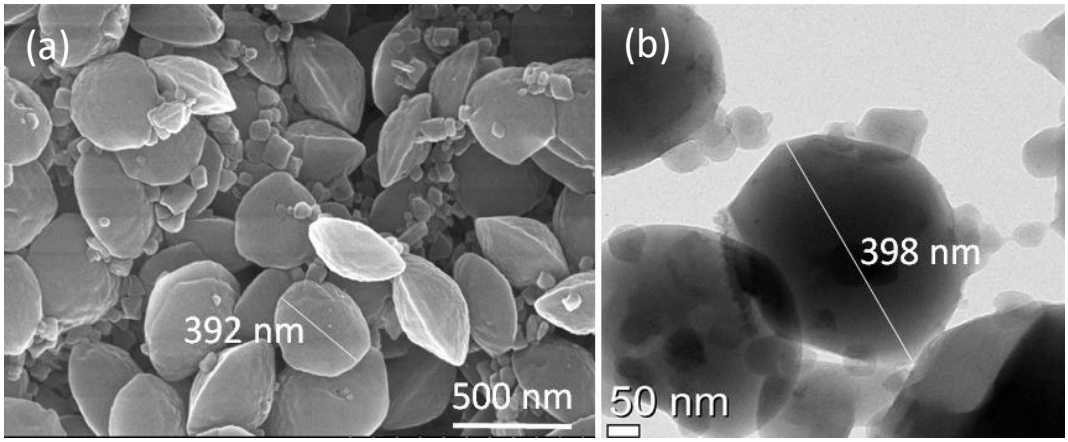

Fig. S3. (a) SEM and (b) TEM images of Cu-Fe-NH_2 MOF bulk powder obtained from ink.

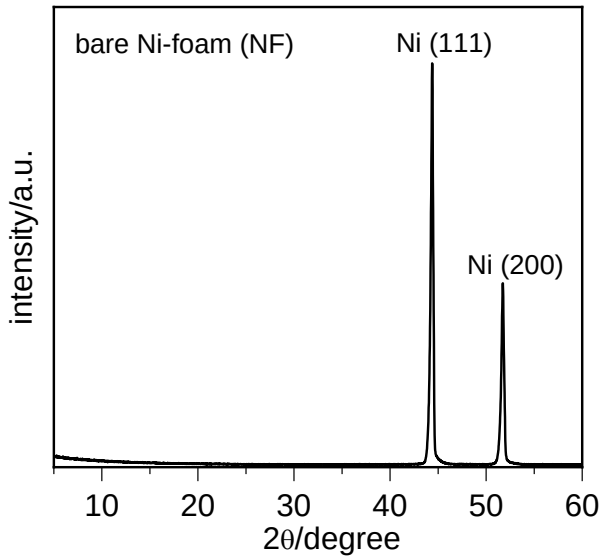

Fig. S4. XRD patterns of bare nickel foam.

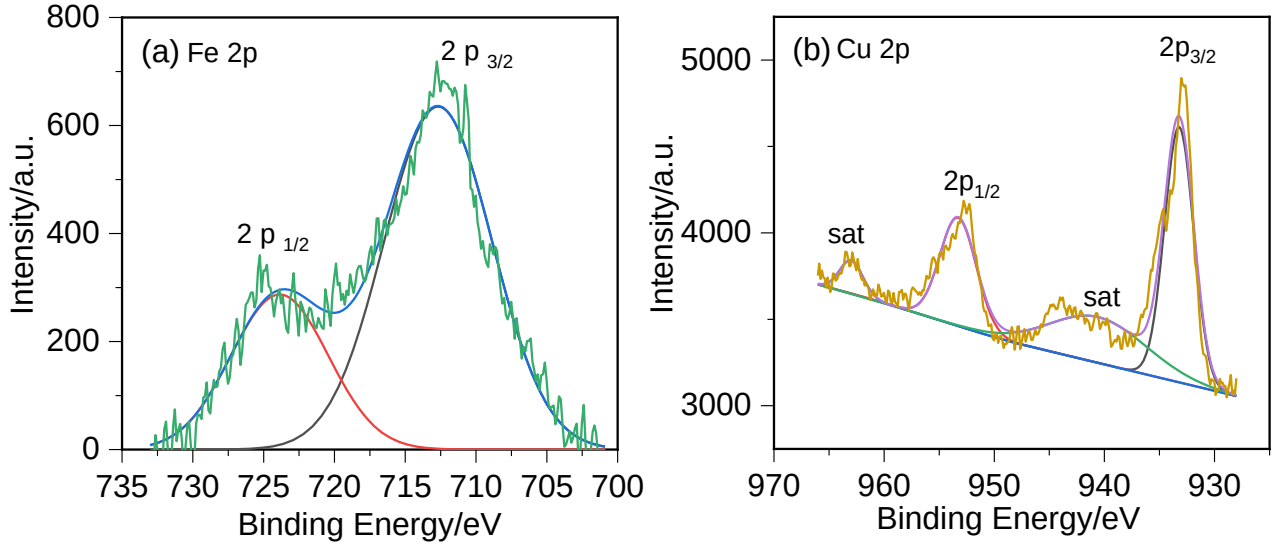

Fig. S5. (a) Fe 2p and (b) Cu 2p XPS core level spectra of Cu-Fe-NH_2 MOF.

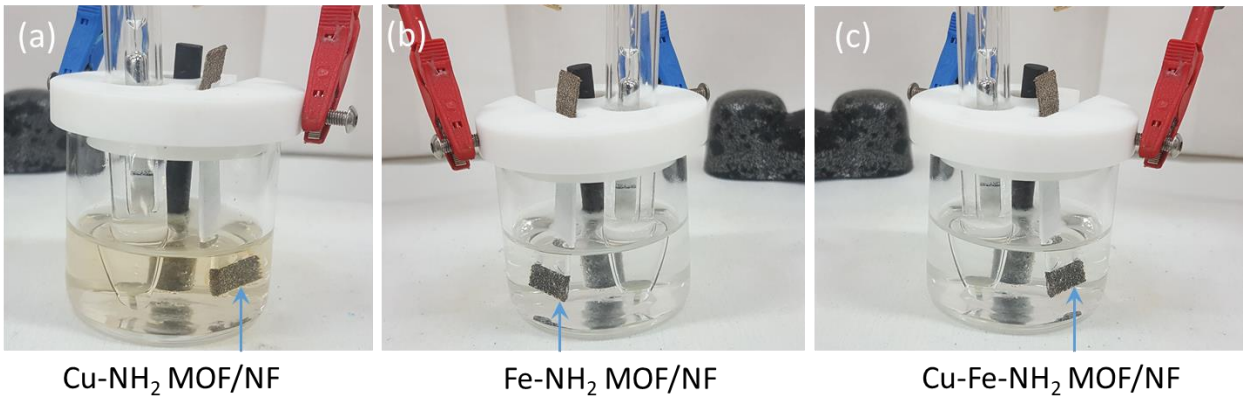

Fig. S6. Photographs of electrolysers constructed with graphite cathodes and (a) Cu-NH_2 MOF/NF, (b) Fe-NH_2 MOF/NF and (c) Cu-Fe-NH_2 MOF/NF anodes in aqueous 1 M KOH electrolyte. A

faint orange color of the electrolyte in "image (a)" indicates that Cu-NH_2 MOF is unstable during electrochemical oxidation reaction.

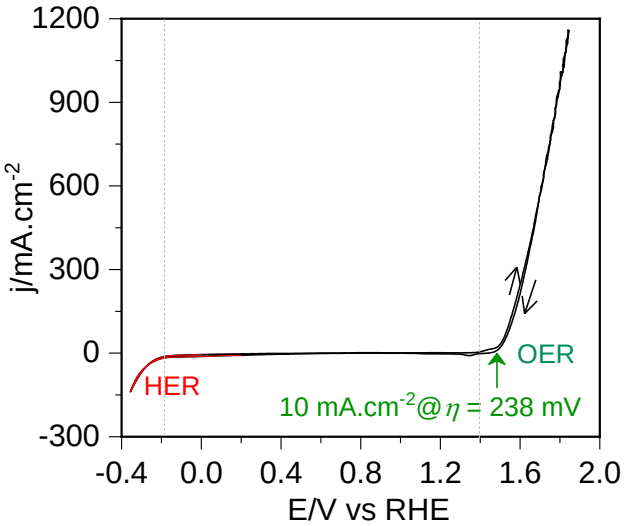

Fig. S7. Cyclic voltammogram of the Cu-Fe-NH_2 MOF/NF electrode in aqueous 1 M KOH electrolyte solution recorded at a scan rate of 5 mV s^{-1}.

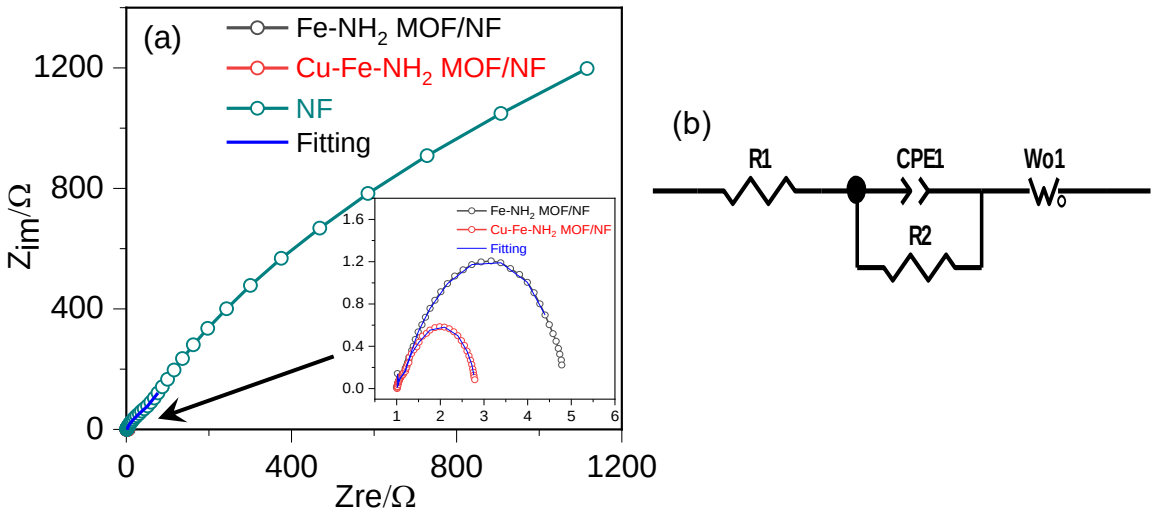

Fig. S8. (a) Nyquists plot obtained from electrochemical impedance spectra of various electrodes in aqueous 1 M KOH electrolyte recorded at a bias of 0.15 V *vs.* RHE. Inset shows the details at low-frequency region indicated by an arrow. (b) An equivalent circuit used to fit Nyquist plots.

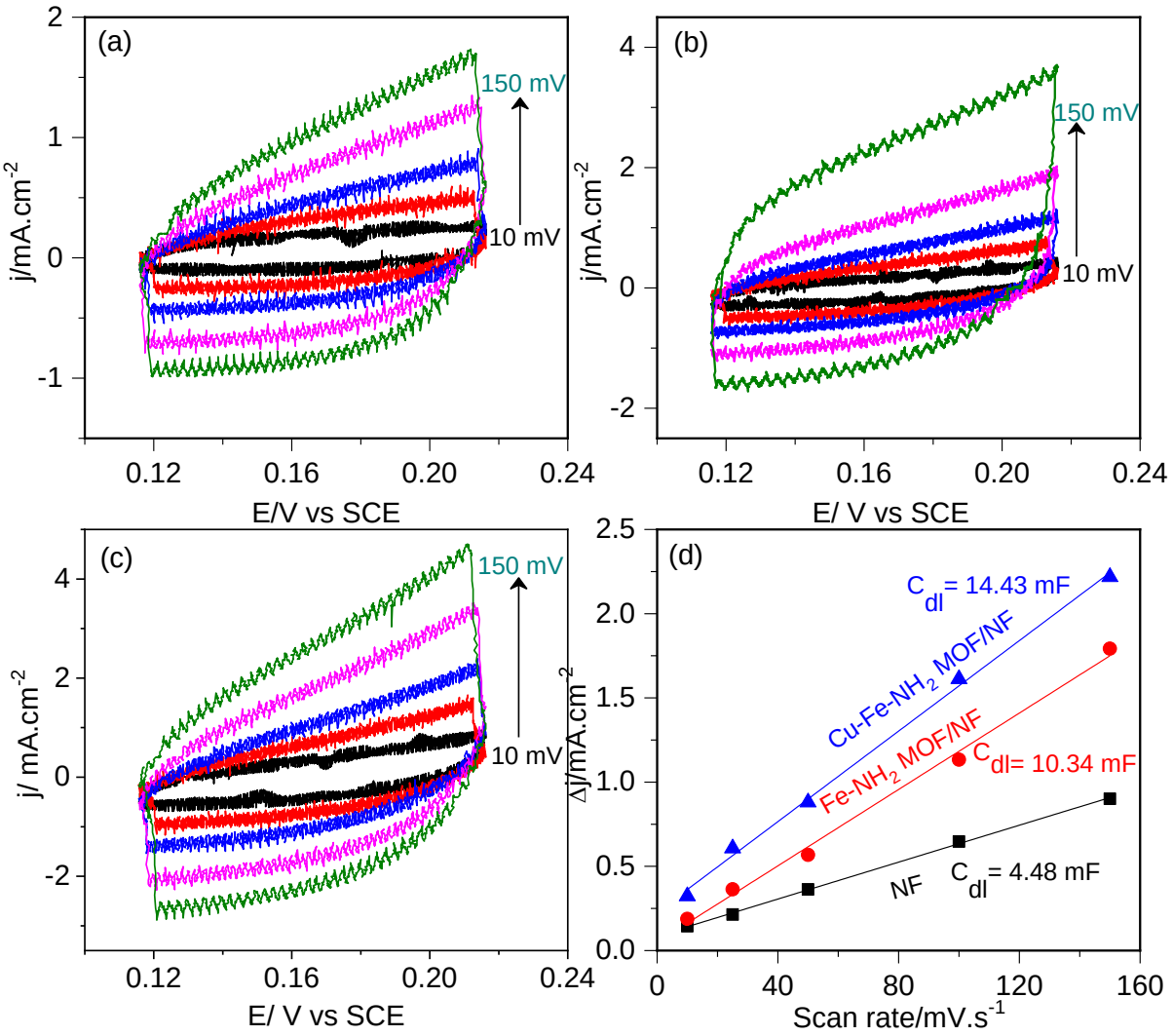

Fig. S9. Cyclic voltammograms of (a) Ni-foam (NF), (b) Fe-NH_2 MOF/NF electrode and (c) Cu-Fe-NH_2 MOF/NF electrode in aqueous 1 M KOH electrolyte recorded in a non-Faradaic region at various scan rates. (d) Average charge current density ($\Delta j = j_{anodic} - j_{cathodic}$) measured at 0.17 V *vs.* SCE as a function of scan rate. Slopes of linear plots of "(d)" were used to determine double-layer capacitance (C_{dl}).

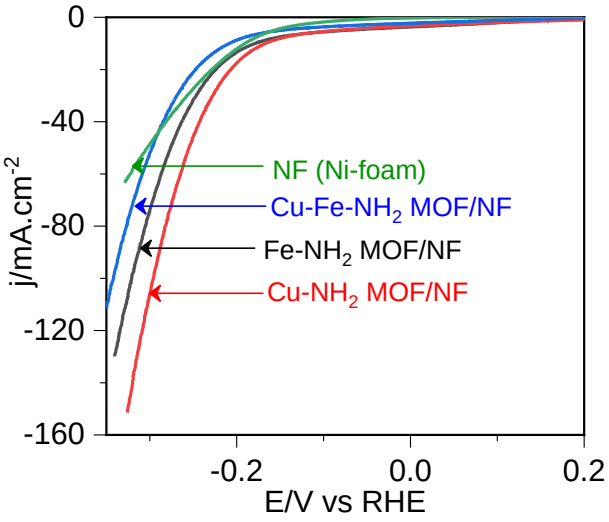

Fig. S10. Linear sweep voltammograms of various electrodes in aqueous 1 M KOH electrolyte recorded at a scan rate of 5 mV s^{-1} to evaluate electrocatalytic HER performance.

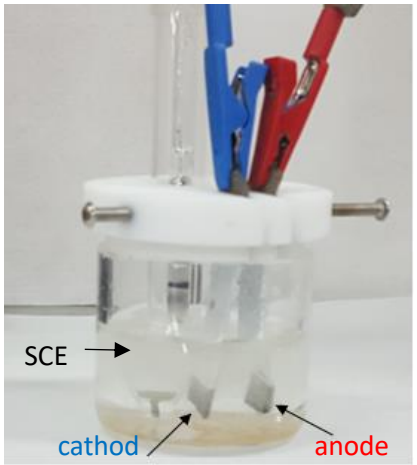

Fig. S11. Photograph of an electrochemical cell with a Cu-Fe-NH_2 MOF/NF‖Cu-Fe-NH_2 MOF/NF cathode/anode assembly in 1 M aqueous KOH electrolyte. This cell was used in linear sweep voltammetry for evaluating HER/OER performance. The same Cu-Fe-NH_2 MOF/NF‖Cu-Fe-NH_2 MOF/NF (cathode‖anode) two-electrode assembly but without SCE reference electrode was used in bulk electrolysis for accessing overall water splitting performance chronopotentiometrically.

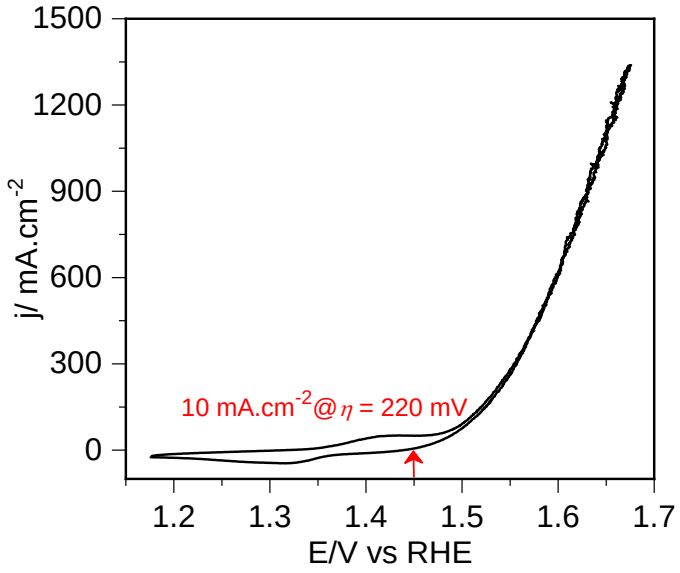

Fig. S12. Cyclic voltammogram of Cu-Fe-NH_2 MOF/NF electrode in an electrochemical cell with the Cu-Fe-NH_2 MOF/NF‖Cu-Fe-NH_2 MOF/NF assembly as shown in "Figure S11". CV was recorded at a scan rate of 5 mV s^{-1}.

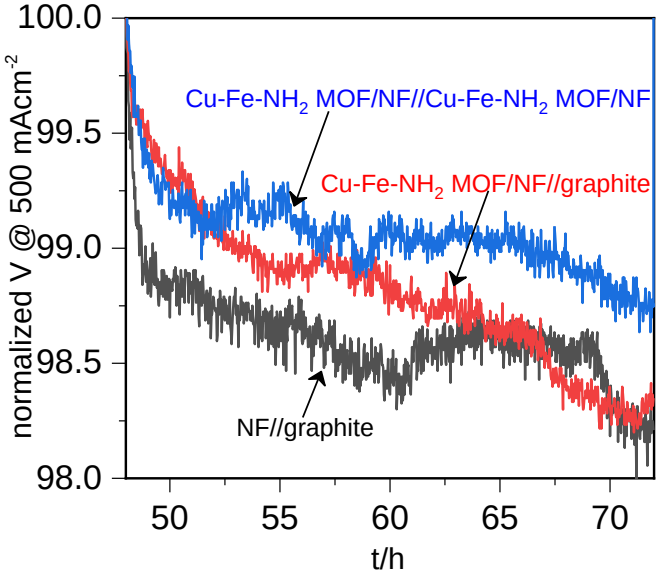

Fig. S13. Normalised chronopotentiometric curves showing cell voltage as a function of time over 24 hours at a bias of 500 mA cm^{-2} using an aqueous 1 M KOH electrolyte solution. Prior to measurement, the same electrodes were used continuously in a bulk electrolysis for 24 h at 100 mA cm^{-2} and again for 24 h 250 mA cm^{-2}, as shown in "Fig. 7a".

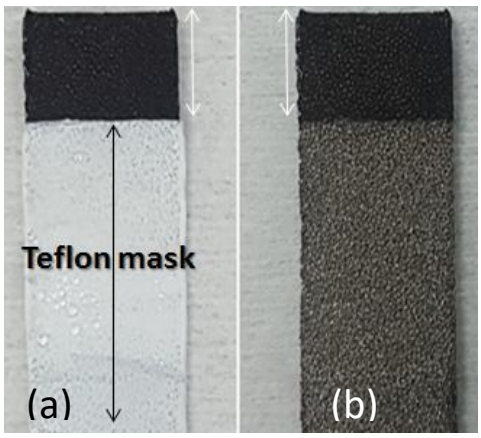

Fig. S14. Photographs of nickel foam after bulk electrolysis in aqueous 1 M KOH electrolyte solution for 24 h at biases of 100, 250 and 500 mA cm^{-2}. The dark black area in (a) and (b) shows an active electrode area used in electrolysis. A sharp border separating the exposed and unexposed regions is visible after removing the Teflon mask. This indicates that the active electrode area remains unchanged even after long-term bulk electrolysis.

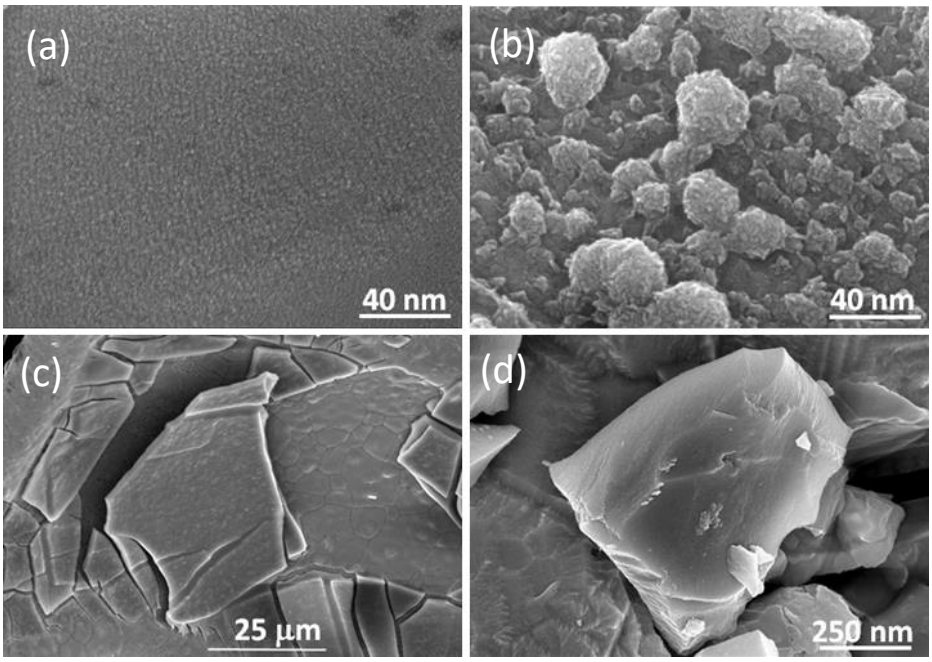

Fig. S15. SEM images of bare nickel foam (NF) and Cu-Fe-NH_2 MOF/NF electrodes before and after bulk electrolysis in aqueous 1 M KOH electrolyte for 24 h at biases of 100, 250 and 500 mA cm^{-2}. NF (a) before and (b) after bulk electrolysis. Cu-Fe-NH_2 MOF/NF electrodes (c) before and (d) after bulk electrolysis.

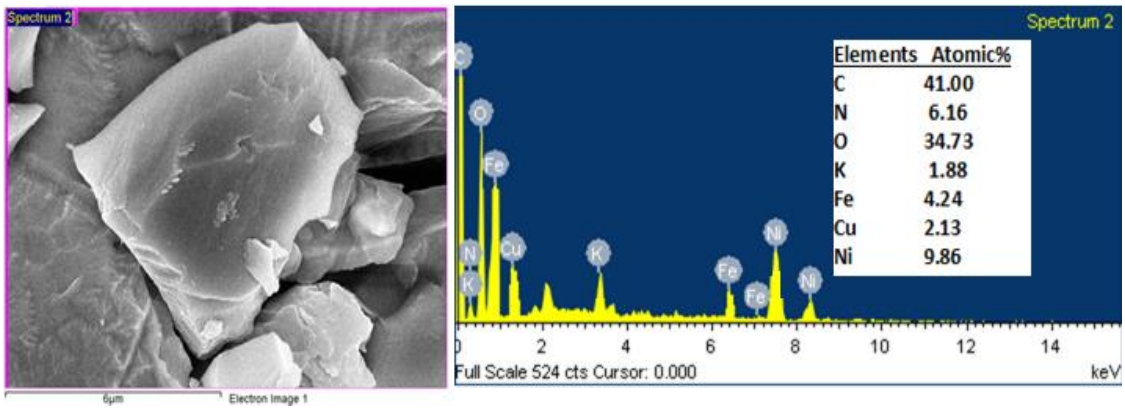

Fig. S16. (a) SEM image and (b) corressponding EDX spetrum of Cu-Fe-NH_2 MOF/NF following bulk electrolysis for 72 h at biases of 100, 250 and 500 mA cm^{-2} in aqueous 1 M KOH electrolyte. Inset in "(b)" shows atomic ratios of various elements present in the electrode.

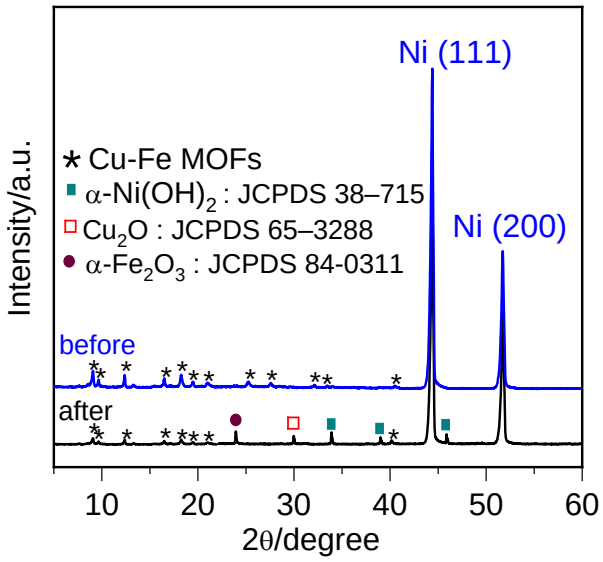

Fig. S17. XRD patterns of Cu-Fe-NH_2 MOF/NF before and after bulk electrolysis in aqueous 1 M KOH electrolyte for 24 h at biases of 100, 250 and 500 mA cm^{-2}.

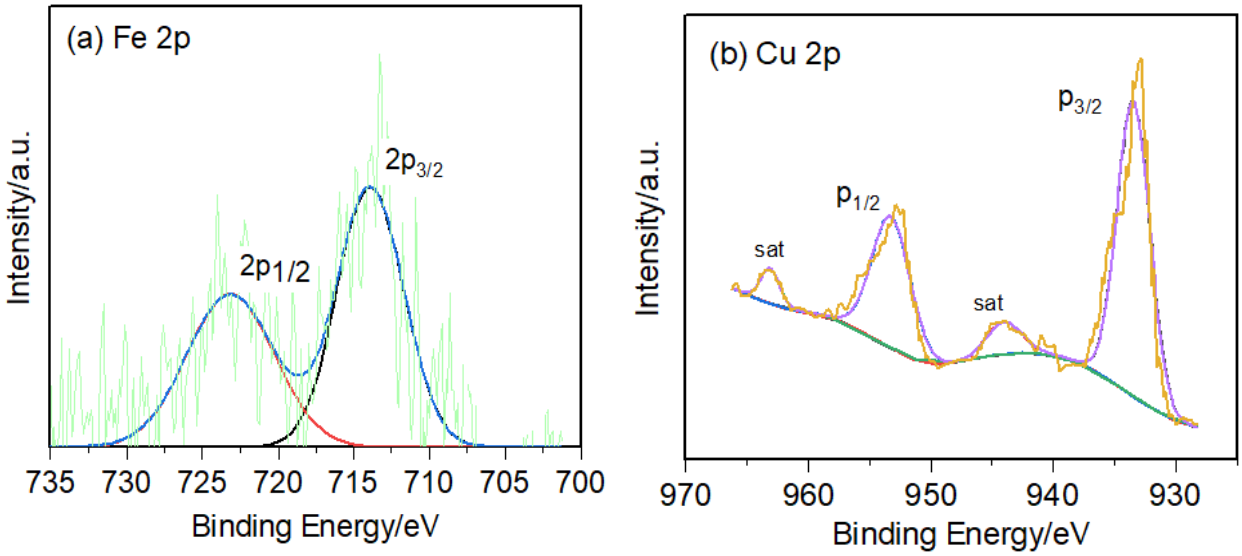

Fig. S18. (a) Fe 2p and (b) Cu 2p XPS core level spectra of the Cu-Fe-NH_2 MOF/NF after the durability test in aqueous 1 M KOH electrolyte for 24 h at biases of 100, 250 and 500 mA cm^{-2}.

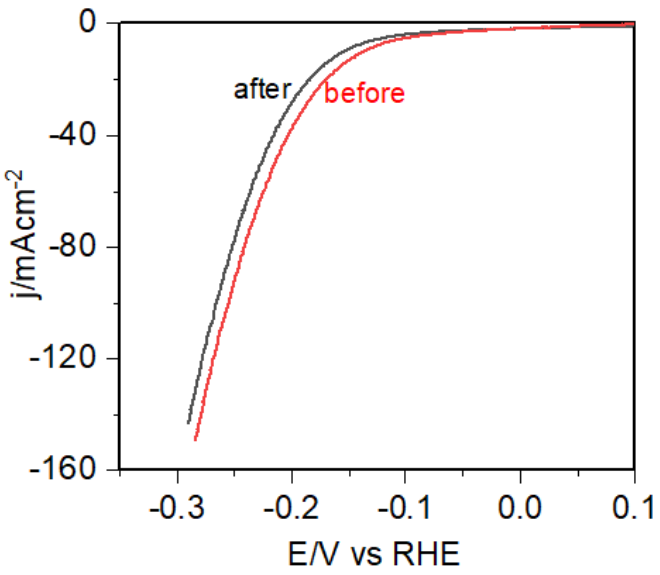

Fig. S19. Linear sweep voltammograms of Cu-Fe-NH_2 MOF/NF before and after bulk electrolysis in aqueous 1 M KOH electrolyte for 24 h at biases 100, 250 and 500 mA cm^{-2}.

Table S1. OER activities of various catalytic electrodes.

	electrode	**Catalyst loading ($mgcm^{-2}$)**	**electrolyte**	**j ($mA\ cm^{-2}$)**	**η_j (mV)**	**Tafel slope ($mVdec^{-1}$)**	**Refs**
1	Cu-Fe-NH_2MOF/NF	0.43	1 M KOH	10 100 250 500 1000	238 170 300 330 390	60.8	**This work**
	Fe-NH_2MOF/NF	1.04		10 100 250 500 1000	260 330 380 470 597	71.9	
	Cu-NH_2MOF/NF	-		100	330	189.8	
	IrO_2(20wt%)-C/NF	1.50		10 100 250 500	262 344 386 504	79.4	

	bare NF			100 250 500	 330 650 720	72.4	
2	NFN-MOF/NF B-NFN-MOF/NF	0.60 0.60	1 M KOH	10 250 500 10 250 500	240 335 360 265 400 495	58.8 61.3	(1)
3	NiCo-UMOFNs/GC NiCo-UMOFNs/Cu-foam	0.20 0.20	1 M KOH	10 10	250 189	42 -	(2)
4	Ir/C-20wt.% NiFe-LDH/CNT	0.20 0.20	1 M KOH 1 M KOH	10 10	290 250	40 31	(3)
	NiFe-MOF/NF	0.30	0.1 M KOH	10	240	34	(4)
5	MIL-53(Fe) -MOF	0.51	1 M KOH	10	219	53.5	(5)
6	Fe/Ni-BTC -MOF@NF	0.50	0.1 M KOH	10	270	47	(6)
7	CS-NiFeCu oxides/NF	-	1 M KOH	10	180	33	(7)
8	CuFe/NF	-	1 M KOH	10	218	62.07	(8)
9	NiFe/$NiCo_2O_4$/NF	-	1 M KOH	10 1200	240 340	38.8	(9)

References:

(1) D. S. Raja, X.-F. Chuah and S.-Y. Lu, *Adv. Energy Mater*., 2018, **8**, 1801065.

(2) S. Zhao, Y. Wang, J. Dong, C.-T. He, H. Yin, P. An, K. Zhao, X. Zhang, C. Gao, L. Zhang, J. Lv, J. Wang, J. Zhang, A. M. Khattak, N. A. Khan, Z. Wei, J. Zhang, S. Liu, H. Zhao and Z. Tang, *Nat. Energy*, 2016, **1**, 16184.

(3) M. Gong, Y. Li, H. Wang, Y. Liang, J. Z. Wu, J. Zhou, J. Wang, T. Regier, F. Wei, H. Dai, *J. Am. Chem. Soc*., 2013, **135**, 8452.

(4) J. Duan, S. Chen and C. Zhao, *Nat. Commun*., 2017, **8**, 15341.

(5) F. L. Li, Q. Shao, X. Huang and J. P. Lang, *Angew. Chem., Int. Ed*., 2018, **57**, 1888.

(6) L. Wang, Y. Wu, R. Cao, L. Ren, M. Chen, X. Feng, J. Zhou and B. Wang, *ACS Appl. Mater. Interfaces*, 2016, **8**, 16736.

(7) P. Zhang, L. Li, D. Nordlund, H. Chen, L. Fan, B. Zhang, X. Sheng, Q. Daniel and L. Sun, Nat Commun., 2018, **9**, 381.

(8) A. I. Inamdar, H. S. Chavan, B. Hou, C. H. Lee, S. U. Lee, S. N. Cha, H. Kim, and H. Im, *Small*, 2019, **16**, 1905884.

(9) C. Xiao, Y. Li, X. Lu, and C. Zhao, *Adv. Funct. Mater*. 2016, **26**, 3515.

Table 2. Impedance parameters extracted from fitting the Nyquist plots shown in Fig. S8.

Element	**Fe-NH_2 MOF/NF**	**Cu-Fe-NH_2 MOF/NF**	**NF**
$R_s(\Omega)$	1.027	0.963	1.154
$R_{ct}(\Omega)$	4.309	1.916	496.800
CPE(μF)	0.633	0.665	0.769
$Z_W(\Omega)$	0.557	0.066	2.481